IEEE Access
Multidisciplinary | Rapid Review | Open Access Journal

Received January 21, 2022, accepted January 29, 2022, date of publication February 7, 2022, date of current version February 15, 2022.

Digital Object Identifier 10.1109/ACCESS.2022.3149895

A Novel Dual Rotor Permanent Magnet Flux Switching Generator for Counter Rotating Wind Turbine Applications

WASIQ ULLAH, (Graduate Student Member, IEEE), FAISAL KHAN, (Member, IEEE), AND SHAHID HUSSAIN, (Graduate Student Member, IEEE)

Department of Electrical and Computer Engineering, COMSATS University Islamabad, Abbottabad Campus, Abbottabad 22060, Pakistan

Corresponding author: Wasiq Ullah (wasiqullah014@gmail.com)

ABSTRACT In this paper counter rotating (CR) dual rotor permanent magnet flux switching generator (CR-DRPMFSG) is designed and relatively studied with co-rotating DRPMFSG (CoR-DRPMFSG) for wind turbine applications. The developed CR-DRPMFSG and CoR-DRPMFSG share same stator linked with flux bridge which provide flux route. A comprehensive relative assessment of both CR-DRPMFSG and CoR-DRPMFSG are presented with static attributes, over-load, and over-speed capability for generating output voltage, output current, output power, power density, losses, and efficiency. Comparative study with static characteristics illustrates that developed CR-DRPMFSG shows 34.34% elevated phase flux which improve output power, cumulative output torque is improved by 23.86%, and suppressed cogging torque by 66.87% at CoR-DRPMFSG that results lower pulsation in instantaneous torque. Furthermore, a detailed performance analysis is investigated with different number of armature winding turns per phase and combined over-load and over-speed capability. Study discloses that in contrast with CoR-DRPMFSG, counterpart CR-DRPMFSG offer 27.17% higher output power that results 1.25 times power density with a good voltage regulation factor of 18.67%. In additional, despite of 2.27% improvement of efficiency in case of phase winding turns analysis and 4.81% increase in over-load and over-speed capability, contour efficiency map unveils that CR-DRPMFSG offer wide range of higher efficiency operating region during over-load and over-speed condition accompany with stable voltage profile with load variation.

INDEX TERMS Flux switching machines, ferrite permanent magnet, counter rotation, wind turbines, wind power generator, wind power application.

I. INTRODUCTION

The prospective growth in necessity and protection of the natural environment dictating the global warming compels to rise the expansion of renewable energy i.e., fuel cell, geothermal, solar energy, biomass plant, tidal energy, and wind turbines for wind energy. From the above-mentioned renewable energies, wind power is plenty in nature, as a consequence expansion of wind energy ruled net renewable power generating capacity in the past decades therefore, believed as quickest developing renewable energy resource. In contrast with non-renewable energy, wind energy power arose as cost-effective and viable renewable energy resource for wind energy power production with installed power of 744 GW at the ending of 2020 [1]. This encourages researcher for engrossment in structure of wind energy power production with varying power scale.

Wind energy power plants adopted various sorts of AC generators such as asynchronous generator, induction generator, field excited synchronous generator, permanent magnet synchronous generator, and permanent magnet flux switching generator (PMFSG). In contrast with field excited synchronous generator and induction generator, permanent magnet synchronous generator produces more power therefore, favour in wind energy systems. Based on position of permanent magnet, generators for wind power applications are categorized as rotor permanent magnet generator i.e., surface mounted permanent magnet (SPM) generator and stator permanent magnet generator.

PMFSG is most common example of stator permanent magnet generator which housed armature winding/field winding and permanent magnet on stator leave behind a

The associate editor coordinating the review of this manuscript and approving it for publication was R. K. Saket.

robust rotor which is developed from the stack of laminated sheets [2]–[6]. PMFSG feature robust rotor and compact stator structure, therefore, exhibits sinusoidal back-EMF, elevated power density, and efficiency. Despite of brushless function, PMFSG offers excellent stator cooling and comparatively improved voltage regulation. Comparative examination of rotor permanent magnet machines with flux switching generators (FSGs) unveil that due to allocation of thermal sources (winding and permanent magnet) on stator, FSGs presents improved heat dissipation, therefore, reduce permanent magnet irreversible demagnetization issues and ease in cooling system, thus, overall machine reliability is enhanced [7]. In additional, in comparison with distributed winding connection, FSGs with non-overlapped single tooth concentrated winding connection inherit least mutual flux coupling with other phase winding, thus, exhibits fault tolerant ability [8].

PMFSG combines improved efficiency, power and torque density feature of permanent magnet machines and robust rotor structure like switched reluctance machine (SRM) therefore, enhance machine reliability and wide speed range performance. Thus, over the past decades several PMFSG of different structures have been studied.

Based on flux flow direction, author in [9] investigated axial flux machine whereas transverse flux machine is studied in [10] and permanent magnet flux switching machines (PMFSMs) with segmented consequent pole is thoroughly investigated in [11]–[14]. In addition to flux flow nature, stator permanent magnet machine was examined with various stator structure and position of rotor i.e., inner rotor [15], [16], outer rotor [17], [18], and dual rotor configuration [19], [20] for improve power density. Inner rotor topologies of PMFSG offers direct coupling of turbine blades with rotor with more pole number due to accessible inner area however, available inner rotor area utilization is very poor [21], [22]. To achieve higher power density and efficiently utilizes the existing area, double rotor FSG are proposed [23], [24]. Moreover, concept of counter rotation is extended in wide range of generator topologies for higher power density. The idea of counter rotation in three phase synchronous generator (SG) was proposed in [25] whereas wind turbine with counter rotation utilizing permanent magnet synchronous generator (PMSG) is developed in [26]. Furthermore, doubly-fed induction generator (DFIG) is proposed in [27] for wind turbine with counter rotation, whereas author in [28] investigates counter rotation by coupling three armatures with outer stator and two rotors however, the aforesaid SG, PMSG and DFIG suffer from production cost and bigger in size than usual for direct-drive wind turbine applications [29]. The aforesaid demerits of DFIG, SG and PMSG are incorporated in double-stator PMFSG utilizing counter rotation wind power application [30], [31].

Compared with single sided PMFSG, dual stator design not only offer higher power but also high reliability [32] however, due to high amount of the rare-earth PM usage, overall machine cost increases and causes PMFSG as expensive

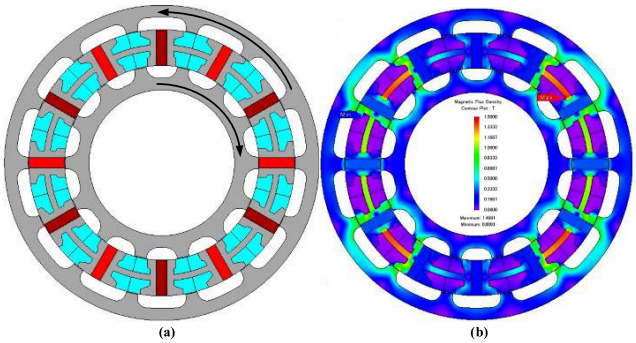

FIGURE 1. Proposed CR-DRPMFSG (a) cross section view and (b) magnetic flux density contour at rated generating condition.

component for wind power generating system but the problem of PM cost can be tackle utilizing ferrite PMs. However, in double-stator topology counter rotation is obtained utilizing opposite rotation of stator and rotor that result mechanical assembly complexity due to involvement of slip rings and brushes. Despite of above-said complexity the sliding contact associates wear and tear, therefore, involves frequent maintenance. Furthermore, slip ring in double-stator made it brushed machine that suffer from friction losses as well. In additional, due to active/energetic part motion that accommodates permanent magnet and armature winding, influence of centrifugal force on permanent magnets develops that results irreversible demagnetization due to excessive generated heat.

Thus, in this paper a counter rotating dual rotor PMFSG (CR-DRPMFSG) (as shown in Figure. 1) is proposed for counter rotating wind power generation that eliminates the requirements of slip ring, truncating slip ring losses, shortened assembly complexity and reduces PM cost. Since proposed CR-DRPMFSG retain energetic active part static, therefore, suppress dominant irreversible demagnetization issue.

In developed CR-DRPMFSG, both inner and outer rotors are rotated in opposite direction to accomplish counter rotation whereas static energetic part i.e., stator retained stationary therefore, omitting the demands of slip ring thus, retained inherit brushless operation. From Figure. 1(a), it can be clearly seen that for counter rotation, in the developed CR-DRPMFSG, inner rotor rotates in clockwise direction whereas outer rotor rotates anti-clockwise direction that results brushless and gearless counter rotation.

It is worth noting that relative rotational speed with counter rotation increases between two armature that results improved power generation within same stator outer diameter thus, active material utilization is suppressed. In additional, due to sandwiched armature between two rotors, flux follow the shortest path through stator flux bridge that results reduced reluctance as well. It is noteworthy that in contrast with existing dual rotor configuration with same rotational direction (co-rotating), the proposed CR-DRPMFSG offer higher power and flexible design in such a way that it can be operated individually i.e., inner rotor only, outer rotor only,

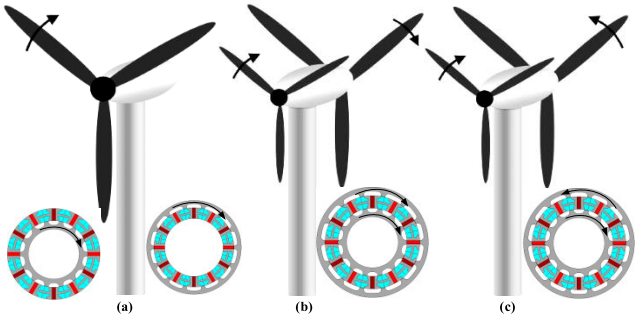

FIGURE 2. DDWT configuration (a) single rotor DDWT (b) DRDDCoRWT and (c) DDDRCRWT.

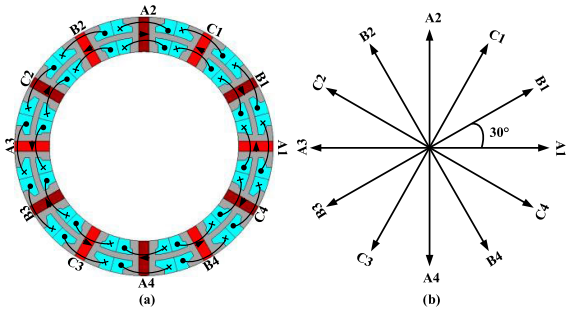

FIGURE 3. EMF phasor diagram and winding connection (a) coil connection in stator slots and (b) Coil and phase EMF phasor.

dual rotor in the same direction and dual rotor in counter rotation. It is noteworthy that in comparison with dual stator topologies, the developed CR-DRPMFSG exhibits merits of dual independent port power transform between inner armature with inner rotor and outer armature with outer rotor. Both ports act like individual generators such that one output can be taken from inner armature and the second output from outer armature whereas total response will be cumulative response of inner and outer armature generators.

In the following, section II discusses direct drive wind turbines, section III investigated proposed CR-DRPMFSG design, static performance analysis is discussed in section IV, generating power performance is investigated in section V, and finally some conclusions are depicted in section V.

II. DIRECT DRIVE WIND TURBINES

Several methods of refining efficiency of energy conversion for kinetic energy of wind into electrical energy have been examined for many years among which direct drives wind turbines (DDWT) are found to be most efficient. In this method, based on rotor spinning and rotational direction, wind turbines are classified as illustrated in Figure. 2.

Figure. 2(a) shows schematics of conventional single rotor DDWT where there is only one rotor that is directly coupled to the shaft of wind turbines. In this configuration, PMFSG are used in two configurations i.e., inner rotor PMFSG or outer PMFSG. Based on comparative study [33], outer rotor PMFSG configuration is most prominent used when high power density is the primal requirements in DDWT.

In the second class of DDWT, dual rotor wind turbine (DRWT) is the emerging technique where two set of rotors rotates in the same direction (co-rotating) as shown in Figure. 2(b) which is term as direct dual rotor direct drive co-rotating wind turbines (DRDDCoRWT). In comparison with the single rotor, DRDDCoRWT results more power density due to rotation of dual rotors that reside in front and rare sides of wind turbines. In this configuration PMFSG is utilized with dual rotor DDWT configuration such that front turbine is attached with one set of rotors whereas the rare side wind turbine is attached to the second rotor set. The cumulative power is the effective power developed by front and rare side wind turbines. Thus, in comparison with single blades turbine system, DRDDCoRWT results twice power density.

In the third class of DDWT, DRWT with two set of rotors rotates in opposite direction i.e., counter-rotating (as shown in Figure. 2(c)), which is term as direct drive dual rotor counter rotating wind turbines (DDDRCRWT). In case of DDDRCRWT, the front side wind turbine rotates in clockwise direction whereas the rare side wind turbine is rotating in counter-clockwise direction [34]. It is noteworthy that both up-stream and down-stream are assumed to be uniform therefore, same rotational speed between front and rare rotor are considered. If upstream flow is made free with undistributed speed, then downstream rotational speed becomes in two parts i.e., distributed, and undistributed resulting variation in rotational speed [35] causing frequency fluctuation.

Comparison of DDDRCRWT power density with single rotor wind turbine reveals that DDDRCRWT produces maximum power density because of dual rotors (front and rare side) that sandwich stator and rotates in counter direction. The resultant power is generated due to front and rare side wind turbines resulting double power generated. In this configuration PMFSG is utilizes with dual rotor or dual stator DDWT configuration. In case of dual stator PMFSG, there are two armatures comprising circumferential magnetized PMs which is sandwich in stator core. In wind turbine, counter rotation with dual stator structure is achieved in such a way that rare turbine blade is connected with rotor whereas both outer and inner stator are connected with front blade of wind turbine. Thus, requires slip ring that increases maintenance cost.

In case of CR-DRPMFSG, the front wind turbine is attached with one set of rotors whereas the rare side wind turbine is attached to the second rotor set. For achieving counter rotation, turbine blades are shaped in such a way that both blades rotate at counter clock-wise direction. Counter rotation in wind turbine system can be achieved in non-direct drive system utilizing co-axial gear box. However, non-direct drive system requires constant maintenance therefore not preferred.

III. PROPOSED CR-DRPMFSG DESIGN

In design prospective, design procedure for motor and generator are different. In case of motor, brushless AC operation

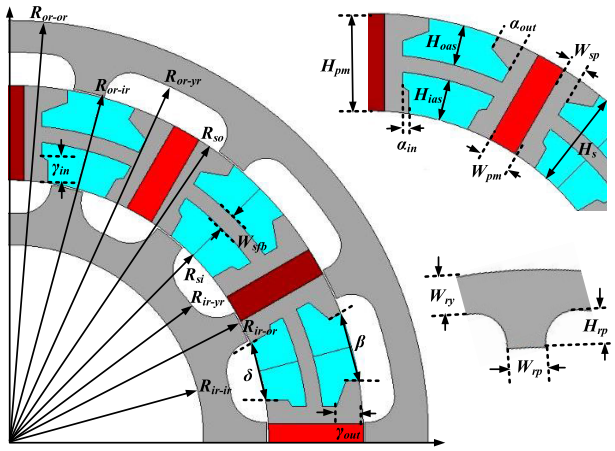

FIGURE 4. Proposed CR-DRPMFSG design parameter.

of $i_d = 0$ is incorporated with defined maximum torque point whereas in case of generator, external connected load is utilized for generator operating condition. In addition, phase angle of applied armature is not controllable in case of generator like motor. Thus, generator optimization is not feasible with brushless AC operating mode. Thus, co-simulation techniques are utilized for generator with external connected load to investigated generator performance. Therefore, generating power performance of the developed generator illustrated in subsequent sections in details both at individual port as well as cumulative response.

Despite of high torque and power density, optimal combination of rotor pole and stator slot combinations are prerequisite to obtain symmetrical phase back electromotive force (EMF). For the proposed design, both inner rotor PMFSG and outer rotor PMFSG allocate to shared stator with the EMF phasor diagram and coil connection as illustrated in Figure. 3. Thus, distribution factor (k_d) with adjacent vector phase shift of 30° becomes [36]

$$k_d = \frac{\sin\left(Qv\alpha/2\right)}{Q\sin\left(v\alpha/2\right)} = 0.966 \tag{1}$$

where $Q = 2$ is least number of MMF vector per phase, $v = 1$ is order of harmonics and $\alpha = 30$ is two adjacent vector angles.

For the proposed CR-DRPMFSG, stator slot (N_s) and rotor pole (N_r) combination with m number of phases are computed as [37]

$$N_s = 2mn_1 \tag{2}$$

$$N_r = N_s \pm n_1 \quad (n_1 = 1, 2, 3\ldots) \tag{3}$$

where, n_1 must be even integer number for even number of m.

Utilizing generator speed (n) and N_r, phase back-EMF frequency under no-load operation can be computed as [38]

$$f = \frac{N_r n}{60} \tag{4}$$

TABLE 1. Design specification of proposed CR-DRPMFSG.

Symbol (Units)	Parameter	Value
R_{or-or} (mm)	Outer rotor outer radius	132
R_{or-ir} (mm)	Outer rotor outer radius	112
R_{or-yr} (mm)	Outer rotor yoke radius	122
R_{so} (mm)	Stator outer radius	111.5
R_{si} (mm)	Stator inner radius	81.5
R_{ir-or} (mm)	Inner rotor outer radius	81
R_{ir-ir} (mm)	Inner rotor inner radius	61
R_{ir-yr} (mm)	Inner rotor yoke radius	71
W_{ry} (mm)	Inner/outer rotor yoke width	10
H_{rp} (mm)	Inner/outer rotor pole height	10
W_{rp} (mm)	Inner/outer rotor pole width	10
W_{pm} (mm)	PM width	9
H_{pm} (mm)	PM height	30
W_{sfb} (mm)	Stator flux bridge width	5
W_{sp} (mm)	Inner/outer stator pole width	5.5
H_{ias} (mm)	Inner armature slot height	12.5
H_{oas} (mm)	Outer armature slot height	12.5
α_{in} (mm)	Inner armature pole shoe width	2
α_{out} (mm)	Outer armature pole shoe width	8
γ_{in} (mm)	Inner armature pole shoe height	8
γ_{out} (mm)	Outer armature pole shoe height	8
δ (mm)	Inner armature slot opening	18.5
β (mm)	Outer armature slot opening	20
N_c (mm)	Number of turns per phase	100
T	Ferrite PM remanence (B_r)	0.4
-	Silicon lamination sheets	35H210
-	Slot filling factor	0.5
L_s (mm)	Stack length	45

Since iron losses are frequency depended therefore, low number of rotor poles are preferred which results reduced frequency of the back-EMF. Therefore, initially 12 stator slot and 14 poles (12S-14P) design is selected.

Proposed CR-DRPMFSG with leading design parameters is shown in Figure. 4. Since proposed CR-DRPMFSG share one stator portion with both inner and outer rotor therefore, some geometric parameters will be shared. Therefore, sizing equations accounts both specific and shared geometric parameters.

For the proposed design, output power (P_{out}) is expressed as [39]

$$P_{out} = mV_r I_r \eta cos\varphi \tag{5}$$

where, V_r, I_r, and η, are rated voltage, rated phase current, efficiency, respectively.

Estimated induced back-EMF for PMFSMs are expressed as

$$e = -N_c \omega \phi_{max} \cos(\omega t) \tag{6}$$

$$\omega = 2\pi n N_r \tag{7}$$

whereas N_c is armature winding turns per phase and ϕ_{max} is maximum air-gap flux density, which are calculated as

$$N_c = \frac{N_s E}{\sqrt{2} n \pi^2 k_L N_r D_g^2 B_{g-max}} \tag{8}$$

$$\phi_{max} = B_{g-max} A_{coil} \tag{9}$$

whereas E, k_L and D_g are rms induced phase back-EMF, aspect ratio and air-gap diameter respectively,

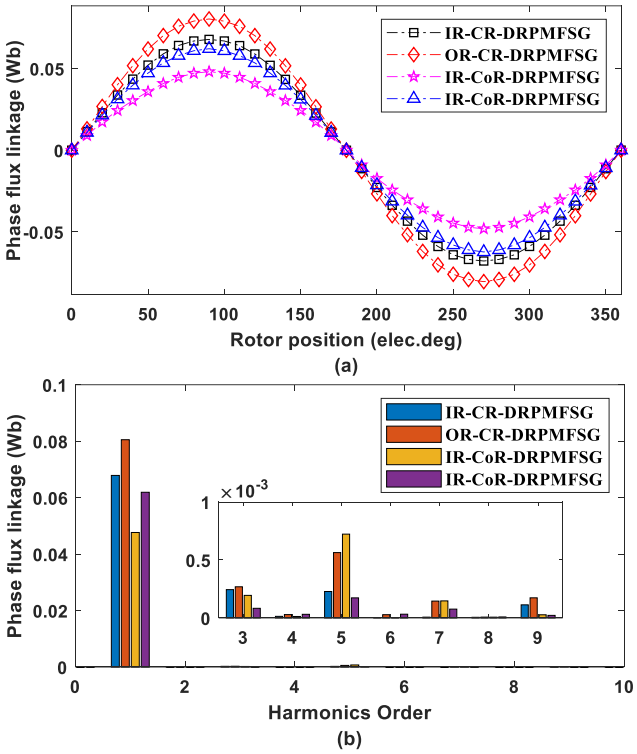

FIGURE 5. Open-circuit phase flux linkage (a) waveform and (b) harmonic spectra.

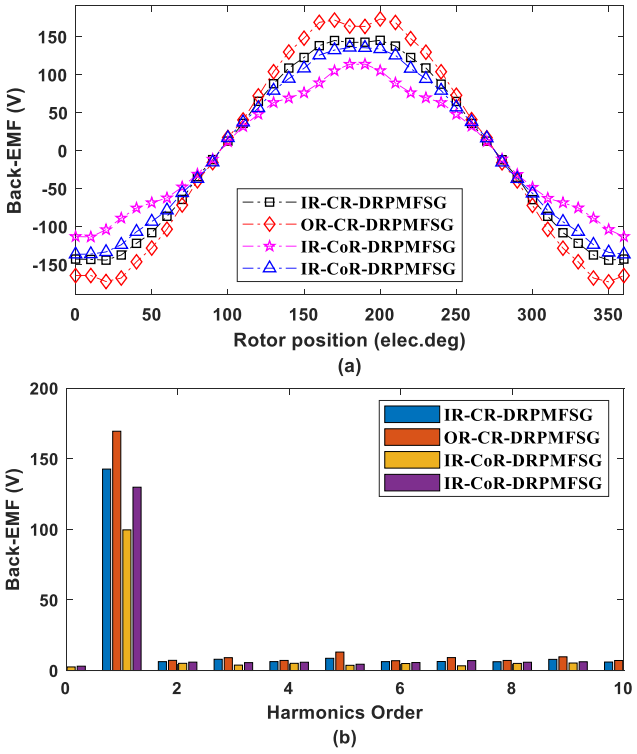

FIGURE 6. Open-circuit phase back-EMF (a) waveform and (b) harmonic spectra.

which are stated as

$$E = \frac{2n\pi^2 N_c N_r L_s D_g B_{g-max}}{\sqrt{2}\, N_s} \tag{10}$$

$$k_L = \frac{L_s}{D_g} \tag{11}$$

$$D_g = \sqrt[3]{\frac{P_{out} N_s}{\sqrt{2}\pi^3 \eta n N_r A_s B_{g-max} k_L k_E cos\,(\phi)}} \tag{12}$$

whereas A_s is electric loading and L_s is active stack length.

Based on the simplified formulation, sub-optimal design specification of proposed CR-DRPMFSG are quantify as

$$R_{or-or} = R_{ir-ir} + R_{ir-or} + 2D_g + R_{so} + R_{or-ir} \tag{13}$$

$$R_{ir-or} = R_{ir-ir} + W_{ry} + H_{rp} \tag{14}$$

$$R_{so} = R_{ir-ir} + W_{ry} + H_{rp} + D_g + H_s \tag{15}$$

$$H_{pm} = H_{ias} + W_{sfb} + H_{oas} \tag{16}$$

$$H_s = H_{ias} + W_{sfb} + H_{oas} \tag{17}$$

$$W_{sfb} = (R_{so} - H_{oas})\text{-}(R_{si} + H_{ias}) \tag{18}$$

To account saturation effects and improve torque calculation and reducing slotting effects that causes cogging torque in the air-gap, optimum design parameters are investigated utilizing finite element analysis (FEA). The final optimum design parameters obtained based on FEA as listed in Table. 1 which is used for detail performance analysis of the CR-DRPMFSG.

IV. STATIC PERFORMANCE ANALYSIS

This section investigates FEA based static performance of proposed DRPMFSG with different rotational direction such as co-rotating and counter rotating. The co-rotating DRPMFSG is termed as (CoR-DRPMFSG) whereas counter rotating is termed as (CR-DRPMFSG). Detailed performance of CoR-DRPMFSG and CR-DRPMFSG are listed in table 2 and illustrated in Figure. 5-7. Note that since the developed proposed model is associated with inner rotor (IR) and outer rotor (OR), therefore, this section discussed individual contribution of each rotor on the performance of CoR-DRPMFSG and CR-DRPMFSG and termed as IR-CoR-DRPMFSG and OR-CoR-DRPMFSG for inner and outer respectively, in case of co-rotating DRPMFSG. Whereas IR-CR-DRPMFSG and OR-CR-DRPMFSG in case of counter rotation. It is noteworthy that static performance is analysed under no-load condition when no armature supply is applied. Induced back-EMF, Phase flux-linkage, and cogging torque are achieved from no-load analysis whereas brushless AC operation is adopted for instantaneous torque profile.

From Figure. 5(a), FEA based open circuit analysis reveals that the highest phase flux linkage (peak-to-peak value of 0.1608 Wb) is offered by OR-CR-DRPMFSG which is due to dominant higher fundamental component and lower higher order harmonics content as shown in Figure. 5(b). After OR-CR-DRPMFSG, the higher flux contribution is associated with the IR-CR-PMFSG which have peak-to-peak value of 0. 1357 Wb whereas the peak-to-peak flux linkage contributed by OR-CoR-PMFSG and IR-CoR-PMFSG are

0.1244 and 0.0961 Wb respectively. Comparative analysis reveals that OR-CR-DR-PMFSG offers 18.34% higher flux than IR-CR-DRPMFSG, 29.09% greater flux than OR-CoR-DRPMFSG and 67.29% more than IR-CoR-DRPMFSG. In addition, when the proposed DRPMFSG is operated, then the cumulative peak-to-peak flux linkage in counter rotation is 0.2963 Wb whereas in co-rotating is 0.2205 Wb. Analysis concludes that in DRPMFSG 34.34% higher phase flux is obtained in case of counter rotation which results an improved performance. This is because, in case of counter rotation, magnitude of the phase flux linkage increases due to the reduction in flux cancellation effect, 3rd, 5th order harmonics reduction and improvement in flux focusing effects.

In open-circuit analysis when no source is applied to the armature winding, back-EMF is induced at the open winding terminals with harmonic spectra is shown in Figure. 6. From Figure. 6(a), it can be clearly seen that both IR-CR-DRPMFSG and IR-CoR-DRPMFSG offer comparatively more symmetrical back-EMF waveform than counterpart OR-CR-DRPMFSG and OR-CoR-DRPMFSG due to least effect of higher order harmonics content. From both waveform and harmonic spectra (as shown in Figure. 6(b)), it can be clearly seen that in case of OR-CR-DRPMFSG and OR-CoR-DRPMFSG, back-EMF waveforms exhibit more harmonics content. It is worth noting that both counter rotation and co-rotation of the rotor have no influence on the harmonics content and purely depend on design structure whereas due to higher phase flux linkage, the back-EMF is improved accordingly.

Because of robust salient rotors, flux modulation effect plays vital role in air-gap magnetic flux density where the field harmonics generated by PM and armature reaction rotate synchronously to generate the torque as shown in Figure. 7. Based on detail investigation of the flux linkage, OR-CR-DRPMFSG offer highest flux linkage which ultimately results higher average torque at the cost of increase in cogging torque (as shown in Figure. 7(a)) and higher torque ripples. Cogging torque analysis reveals that in CR-DRPMFSG, 7.73 Nm cogging torque is contributed by IR-CR-DRPMFSG whereas 13.01 Nm by OR-CR-DRPMFSG whereas in case of CoR-DRPMFSG, 4.66 Nm is contributed by IR-CoR-DRPMFSG whereas 9.22 Nm is offered by OR-CoR-DDRPMFSG. Analysis reveals that rotor rotation has dominant influence on cogging torque. It can be clearly seen that in case of CR-DRPMFSG, peak-to-peak cogging torque is 20.74 Nm whereas CoR-DRPMFSG exhibits peak-to-peak cogging torque of 13.87 Nm which is 66.87% reduced than counterpart. This reduction in cogging torque is due to reduction of dominant slotting effect, thus, offer low vibration and acoustic noise [40].

This increase in the cogging results pulsation in the instantaneous torque waveform (as shown in Figure. 7(b)) in the form of torque ripples. Detail studies unveil that in CR-DRPMFSG, 18.36 Nm of average torque is

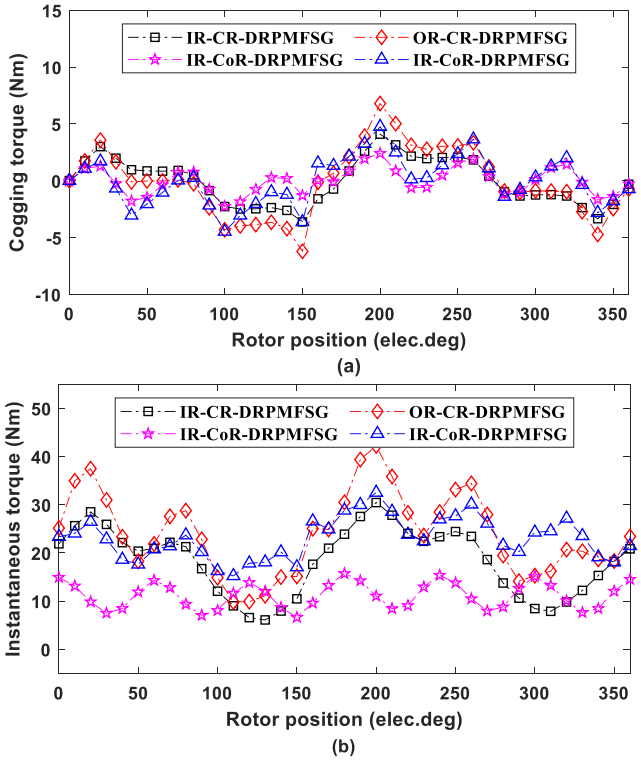

FIGURE 7. Torque performance (a) cogging torque and (b) instantaneous torque.

contributed by IR-CR-DRPMFSG whereas 23.87 Nm by OR-CR-DRPMFSG whereas in case of CoR-DRPMFSG, 11.197 Nm is contributed by IR-CoR-DRPMFSG and 23.026 Nm is offered by OR-CoR-DDRPMFSG.

V. GENERATING POWER PERFORMANCE

Power generating performance under symmetrical external load resistance for CR-DRPMFSG and CoR-DRPMFSG includes losses, output voltage, output current, output power, output power density, efficiency, and voltage regulation capability. In this analysis, initially, number of turns (N_c) are analysed and then proceeded to overload and overspeed capability. It is noteworthy that the results discussed in this section is based on cumulative response (summation of inner and outer armature port) not individual port/rotor.

A. NUMBER OF TURNS

Number of turns are designed carefully so that optimum number of turns are obtained to ensure least voltage regulation and fulfill the rated specification i.e., rms value of 220 V under rated design specification. In design stage, normally 20% of higher margin is secured so that voltage is decrement caused by manufacturing and assembly is avoided. It is noteworthy that higher number of turns are detrimental because it elevates voltage stabilization capability of generators with load variation.

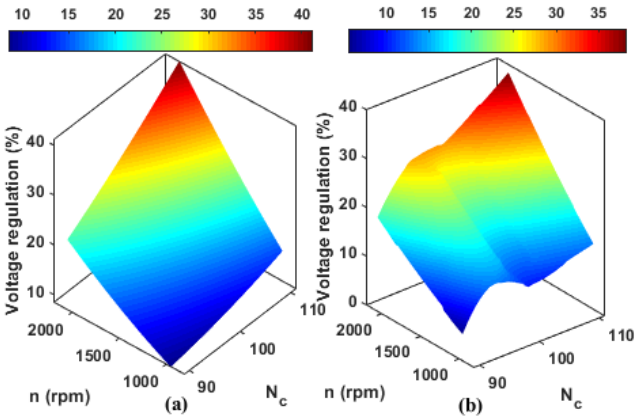

FIGURE 8. Variation of voltage regulation with phase winding and speed in (a) CR-DRPMFSG and (b) CoR-DRPMFSG.

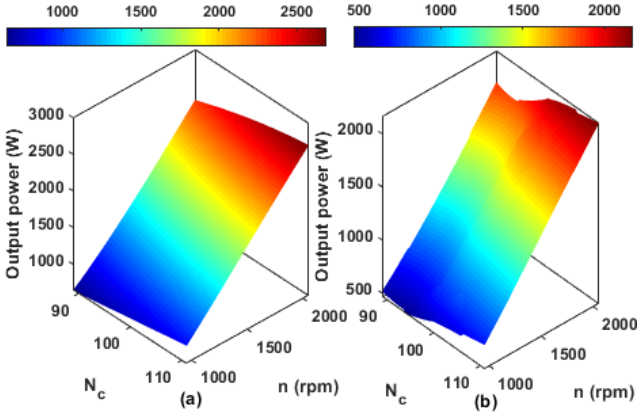

FIGURE 9. Variation of output power with phase winding and speed in (a) CR-DRPMFSG and (b) CoR-DRPMFSG.

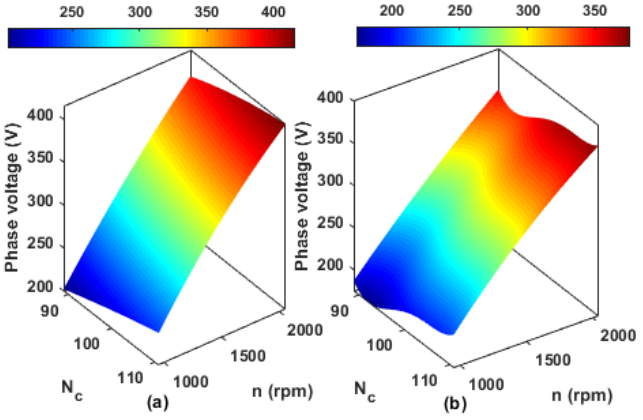

FIGURE 10. Variation of phase voltage with phase winding and speed in (a) CR-DRPMFSG and (b) CoR-DRPMFSG.

The voltage regulation factor of generator with the variation of the load is expressed as [2], [3]

$$U = \left(\frac{E}{V_o} - 1\right) 100\% \tag{19}$$

whereas V_o is the output phase voltage which is computed with the variation of the load changes.

Under symmetrical pure resistive load operation of generator, both the output phase voltage and output phase current are in phase. Considering the influence of phase winding resistance (R_{ph}) and phase reactance (X_s), therefore,

$$E = I_o\sqrt{(R_N + R_{ph})^2 + X_s^2} \tag{20}$$

whereas R_N is the connected load resistance, thus

$$V_o = I_o R_N \tag{21}$$

The voltage regulation factor becomes

$$U = \left(\frac{\sqrt{(R_N + R_{ph})^2 + X_s^2}}{R_N} - 1\right) 100\% \tag{22}$$

Moreover, from section II, it can also be seen that induced back-EMF is also depended on speed at which the rotor rotates which are coupled to the turbines. Thus, a detailed investigation of the effecting factors (number of turns and speed) is thoroughly investigated not only for voltage regulation but also for output phase voltage, phase current, output power, losses and efficiency as shown in Figure. 9 to Figure. 14.

From Figure. 8, it can be clearly seen that voltage regulation factor of both CR-DRPMFSG and CoR-DRPMFSG varies with the variation of the number of turns and speed because phase winding resistance is proportional to number of turns whereas winding reactance is proportional to the square of number of turns. The highest voltage regulation factor reached is 36.08% for CR-DRPMFSG and 39.1% for CoR-DRPMFSG under 2000 rpm and 110 number of turns. Therefore, normalized voltage regulation factor value is decided based on design output power as shown in Figure. 9 and rated output phase voltage as shown in Figure. 10. Analysis reveals that with the voltage regulation margin of 20%, specification power of 1500 W and rated phase voltage is achieved with 100 number of turns per phase winding and speed of 1500 rpm. In this point, CR-DRPMFSG exhibits 18.63% voltage regulation and rated power of 1620 W whereas counterpart CoR-DRPMFSG offer 20.23% voltage regulation and 1284 W rated power. Based on the required specification power, it is evident that under same design parameters and both electrical and magnetic loading, voltage regulation factor is achievable with both CR-DRPMFSG and CoR-DRPMFSG however, the required power level can be achieved with counter rotation only. Comparison of counter rotation with counterpart co-rotation shows that 26.17% higher output power is achievable under counter rotating wind turbines.

Despite of higher output power proposed CR-DRPMFSG offer higher output phase voltage and output phase current as shown in Figure. 10 and Figure. 11, respectively which results higher power and ultimately improve the power density as shown in Figure. 12. Detailed study shows that

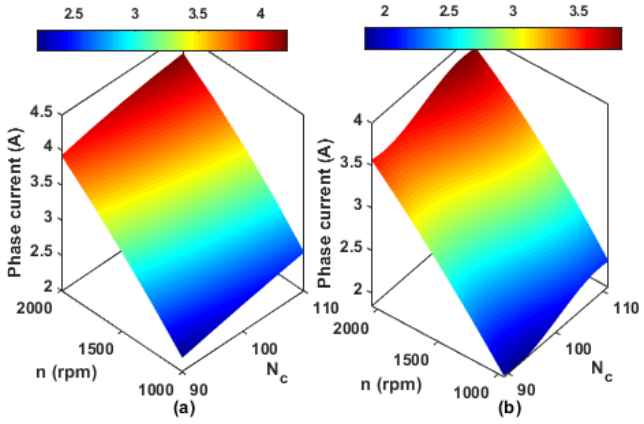

FIGURE 11. Variation of phase current with phase winding and speed in (a) CR-DRPMFSG and (b) CoR-DRPMFSG.

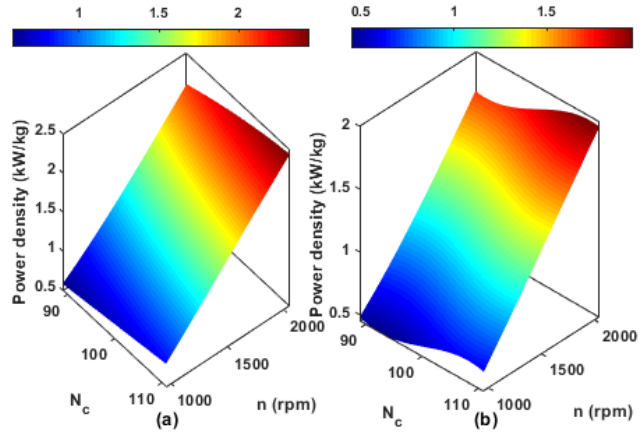

FIGURE 12. Variation of output power density with phase winding and speed in (a) CR-DRPMFSG and (b) CoR-DRPMFSG.

highest power density of 2 kW/kg is obtained with co-rotation whereas counter rotation offers 2.5 kW/kg power density. This shows that counter rotation exhibits power density of 1.25 times in comparison with the co-rotation. Furthermore, at desired specification point (number of turns = 100, and speed = 1500 rpm), power density of 1.47 kW/kg is offered by CR-DRPMFSG whereas 1.17 kW/kg by CoR-DRPMFSG.

Once the desired specification in term of the voltage regulation, output phase current, output phase voltage and output power are obtained with higher power density, both CR-DRPMFSG and CoR-DRPMFS are analyzed in term of the losses and efficiency as shown in Figure. 13 and Figure 14 respectively. Analysis shows that both losses and efficiency greatly vary with number of turns and speed. In case of CR-DRPMFSG, losses directly increase with the increase in number of turns and speed. This same variation pattern in reverse shaped is absorbed in efficiency whereas for CoR-DRPMFSG, in speed lower than 1500 rpm, the losses show increasing behaviour but at higher speed, the losses first increase and then decreases which greatly effects higher

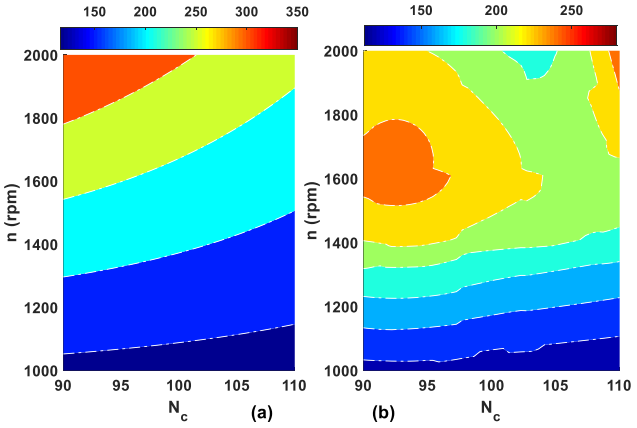

FIGURE 13. Variation of losses with phase winding and speed in (a) CR-DRPMFSG and (b) CoR-DRPMFSG.

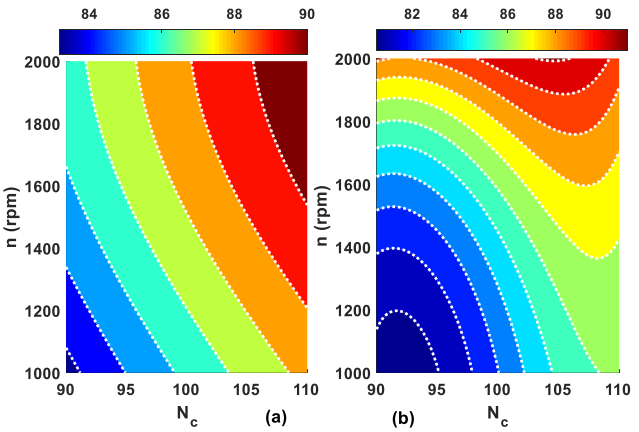

FIGURE 14. Variation of efficiency with phase winding and speed in (a) CR-DRPMFSG and (b) CoR-DRPMFSG.

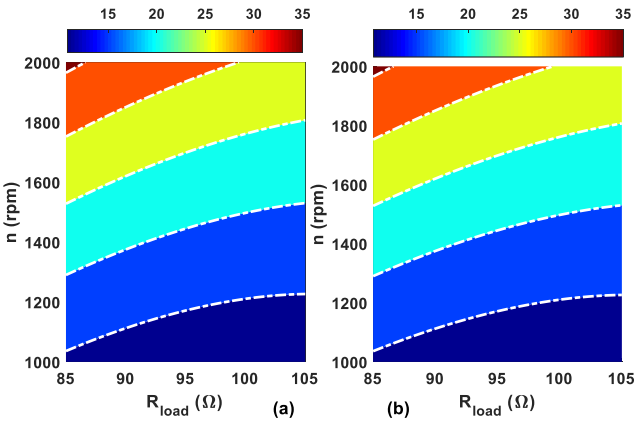

FIGURE 15. Influence of variable resistive load and speed on voltage regulation factor of (a) CR-DRPMFSG and (b) CoR-DRPMFSG.

efficiency regions. A close look of the efficiency counter reveals that CR-DRPMFSG offer flexible wide range boundary under higher efficiency region whereas a small higher efficiency operating point exist in CoR-DRPMFSG at higher speed regions which are not desirable for wind power

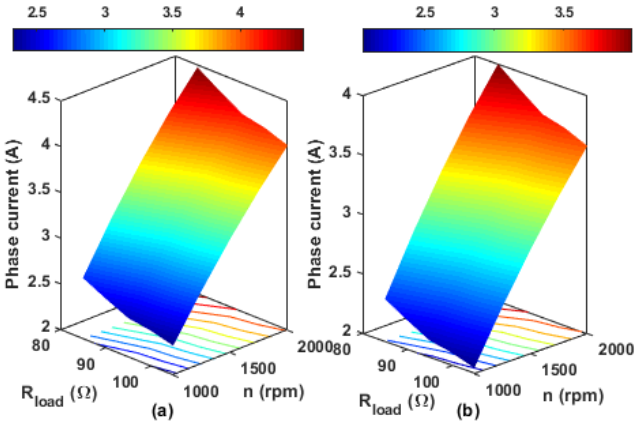

FIGURE 16. Influence of variable resistive load and speed on phase current of (a) CR-DRPMFSG and (b) CoR-DRPMFSG.

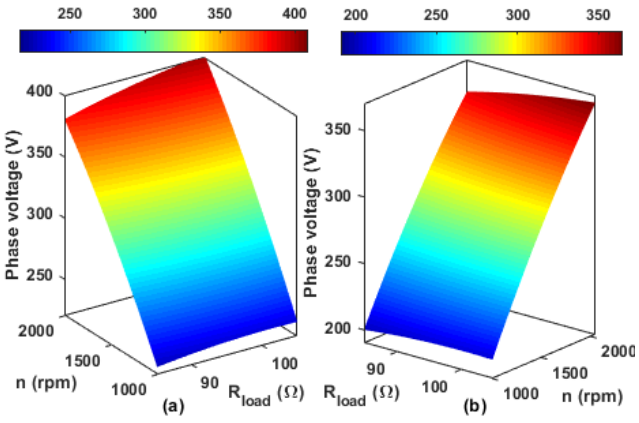

FIGURE 17. Influence of variable resistive load and speed on phase voltage of (a) CR-DRPMFSG and (b) CoR-DRPMFSG.

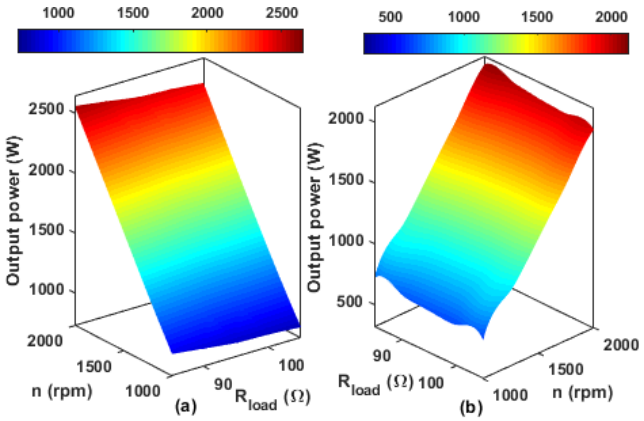

FIGURE 18. Influence of variable resistive load and speed on output power of (a) CR-DRPMFSG and (b) CoR-DRPMFSG.

turbines. It is worth noting that both CR-DRPMFSG and CoR-DRPMS offer maximum efficiency of 90% but with different operating boundaries. In case of CR-PMFSG, highest efficiency of 87% is achieved at the operating level whereas counterpart CoR-DRPMFSG exhibits efficiency of 83%.

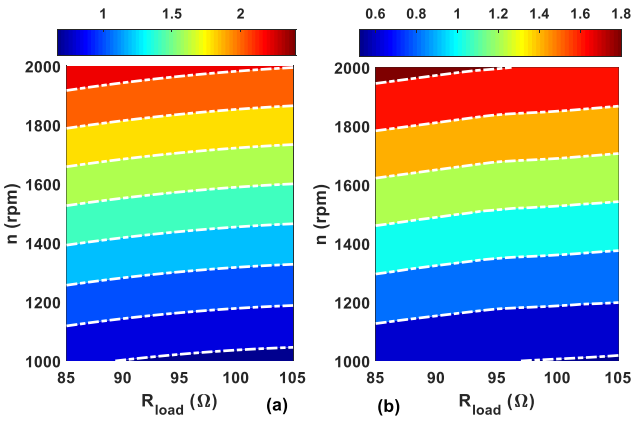

FIGURE 19. Influence of variable resistive load and speed on power density (*kW*/*kg*) of (a) CR-DRPMFSG and (b) CoR-DRPMFSG.

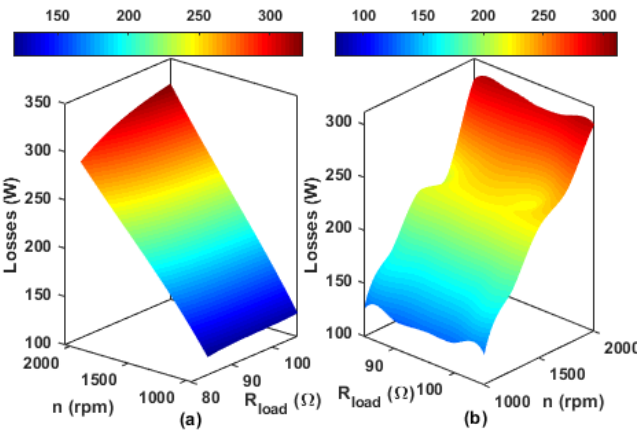

FIGURE 20. Influence of variable resistive load and speed on losses of (a) CR-DRPMFSG and (b) CoR-DRPMFSG.

Furthermore, highest efficiency of 90% in CR-DRPMFSG is achieved at number of turn greater than 100 and speed more than 1200 rpm whereas in CoR-DRPMFSG it is obtained only at speed higher than 1800 rpm. It is noteworthy that at the operating level, CR-DRPMFSG offers 4.81% higher efficiency than counterpart CoR-DRPMFSG.

B. OVER-LOAD AND OVER-SPEED CAPABILITY

This section illustrates coupled overload and overspeed capability for detailed investigation of generating power performance of both CR-DRPMFSG and CoR-DRPMFSG, so that influence of the load variation with varies speed are analyzed in detail. In case of overspeed capability, the design is operated at higher speed than the rated whereas in case of the overload capability, analysis is performed with varying load profile under key performance indicators i.e., voltage regulation, output current, output phase voltage, output power, power density, loss, and efficiency with various connected resistive load. It is worth mentioning that in case of overload capability, analysis mainly focus on symmetrical three phase pure resistive load (R_{load}) only.

Figure. 15 shows contour map of voltage regulation factor of CR-DRPMFSG and CoR-DRPMFSG with variation of connected resistive load. It can be observed that voltage regulation factor co-rotation and counter rotation have no influence on voltage regulation, and it is totally dependent on the connected load and operating speed. It can be clearly seen that voltage regulation increases with the increase in speed as well as connected load which is in accordance with the previous discussion. Figure. 16 and Figure. 17 show RMS values of the output voltage with RMS output current respectively for both CR-DRPMFSG and CoR-DRPMFSG with varies load and speed. Output voltage stability under different resistive load is analyzed from the curve slope. A detailed investigation reveals that slop of the curve for CR-DRPMFSG is higher compared to counterpart CoR-DRPMFSG thus indicates higher voltage variation with the resistive load variation therefore exhibits advantages of maintaining more stable voltage.

The variation of output power and power density is display in Figure. 18 and Figure. 19, respectively. Analysis illustrates that both CR-DRPMFSG and CoR-DRPMFSG exhibits good response in term of the output power and power density under overload and overspeed capability. Comparative analysis of CR-DRPMFSG and CoR-DRPMFSG shows that proposed CR-DRPMFSG offer comparatively better performance. Analysis of output power shows that CR-DRPMFSG offers 1.25 times higher power at overload and overspeed capability. Similarly, power density analysis shows that CR-DRPMFSG exhibits 22.2% higher power density than counterpart CoR-DRPMFSG.

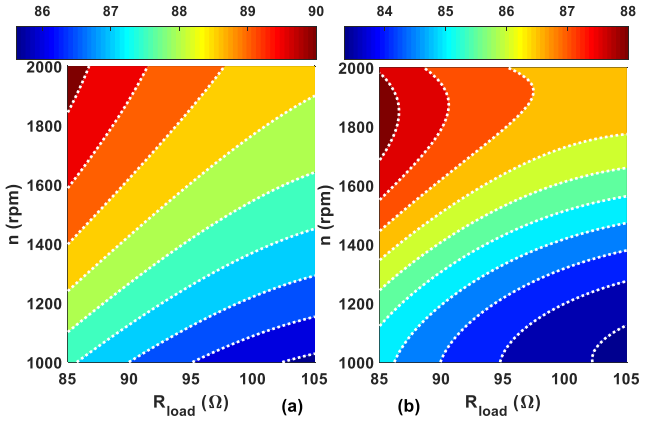

FIGURE 21. Influence of variable resistive load and speed on efficiency of (a) CR-DRPMFSG and (b) CoR-DRPMFSG.

In key performance indicator, the overload and overspeed capability on losses and efficiency of both CR-DRPMFSG and CoR-DRPMFS is illustrated as shown in Figure. 20 and Figure 21, respectively. Detailed investigation of loss for CR-DRPMFSG reveals that as soon as the connected load changes corresponding losses are changes. Similarly, with the change in the rotor speed, the corresponding frequency increases results an increase in the losses which is same for CoR-DRPMFSG also. Despite of the rotor rotation overall losses increase due to the increase in the core losses at higher frequency which greatly effects efficiency however, with the variation of the connected the losses greatly varies. In case of CR-DRPMFSG, with the increase in the connected resistive load, the losses slightly increase whereas the growth rate of losses for CoR-DRPMFSG is comparatively higher. Since losses variation have slight influence, this results higher overall efficiency and wide operating range in comparison with CoR-DRPMFSG. Quantitative analysis reveals that despite of wide operating range proposed CR-DRPMFSG offers 2.27% higher efficiency than CoR-DRPMFSG.

TABLE 2. Generator rating and quantitative comparsion @ speed = 1500 rpm, $N_c = 100$, $R_L = 96.8\Omega$.

Parameters (Units)	CoR-DRPMFSG		CR-DRPMFSG	
	IR	OR	IR	OR
ψ_{pp} (Wb)	0.096	0.125	0.136	0.161
ψ_{thd} (%)	1.61	0.394	0.5275	0.844
E_{mf} (V)	226.88	270.95	289.72	345.89
T_c (Nm)	4.65	9.24	7.73	13.00
T_a (Nm)	11.19	23.02	18.35	23.97
ΔV (%)	35.50	35.49	16.54	23.57
V_r (V)	130.34	153.23	141.45	168.27
I_r (A)	1.39	1.57	1.46	1.73
P_r (W)	543.52	721.71	619.66	873.32
η (%)	71.02	76.49	73.65	79.78
l (W)	221.74		221.3	

Finally, a comprehensive comparison of the key metric function i.e., phase flux linkage (ψ_{pp}), flux THD (ψ_{thd}), back EMF (E_{mf}), cogging torque (T_c), average torque (T_a), voltage regulation (ΔV), rated RMS current (I_r), rated EMS voltage (V_r), rated output power (P_r), losses (l), and efficiency (η) for both CoR-DRPMFSG and CR-DRPMFSG incorporating contribution of both Inner rotor (IR) and Outer Rotor (OR) contribution are investigated as listed in table 2. It can be clearly seen that CR-DRPMFSG offers comparatively better performance at both IR and OR than counterpart CoR-DRPMFSG.

VI. CONCLUSION

In this paper CR-DRPMFSG is designed and comparatively analyzed with CoR-DRPMFSG for wind turbine applications. Detailed analyses are performed under static characteristics, overload, and over-speed capability for power generating performance. Static characteristics analysis illustrates that CR-DRPMFSG exhibits 34.34% higher flux which improve output power, cumulative output torque is improved by 23.86%. Furthermore, from detailed study with different number of armature winding turns per phase and coupled overload and overspeed capability, analysis concludes that in comparison with CoR-DRPMFSG counterpart CR-DRPMFSG offer 27.17% higher output power that results 1.25 times power density at a good voltage regulation factor of 18.67%. Moreover, despite improvement in efficiency under overload and overspeed capability, contour efficiency map unveils that CR-DRPMFSG offer wide range of higher

efficiency operating region accompany with stable voltage profile with the load variation. Effectiveness of the proposed CR-DRPMFSG will be test and validated in the future with experimental prototype.

REFERENCES

[1] WWEA. (2021). Accessed: Nov. 9, 2021. [Online]. Available: https://wwindea.org/information-2/statistics-news/
[2] L. Shao, W. Hua, F. Li, J. Soulard, Z. Q. Zhu, Z. Wu, and M. Cheng, "A comparative study on nine- and twelve-phase flux-switching permanent-magnet wind power generators," *IEEE Trans. Ind. Appl.*, vol. 55, no. 4, pp. 3607–3616, Jul. 2019.
[3] L. Shao, W. Hua, J. Soulard, Z.-Q. Zhu, Z. Wu, and M. Cheng, "Electromagnetic performance comparison between 12-phase switched flux and surface-mounted PM machines for direct-drive wind power generation," *IEEE Trans. Ind. Appl.*, vol. 56, no. 2, pp. 1408–1422, Mar. 2020.
[4] J. Ojeda, M. G. Simoes, G. Li, and M. Gabsi, "Design of a flux-switching electrical generator for wind turbine systems," *IEEE Trans. Ind. Appl.*, vol. 48, no. 6, pp. 1808–1816, Nov./Dec. 2012.
[5] A. S. Thomas, Z. Q. Zhu, and G. W. Jewell, "Comparison of flux switching and surface mounted permanent magnet generators for high-speed applications," *IET Elect. Syst. Transp.*, vol. 1, no. 3, pp. 111–116, Sep. 2011.
[6] F. Li, W. Hua, M. Tong, G. Zhao, and M. Cheng, "Nine-phase flux-switching permanent magnet brushless machine for low-speed and high-torque applications," *IEEE Trans. Magn.*, vol. 51, no. 3, pp. 1–4, Mar. 2015.
[7] Z. Q. Zhu and J. T. Chen, "Advanced flux-switching permanent magnet brushless machines," *IEEE Trans. Magn.*, vol. 46, no. 6, pp. 1447–1453, Jun. 2010.
[8] M. Cheng, W. Hua, J. Zhang, and W. Zhao, "Overview of stator-permanent magnet brushless machines," *IEEE Trans. Ind. Electron.*, vol. 58, no. 11, pp. 5087–5101, Nov. 2011.
[9] W. Zhao, T. A. Lipo, and B.-I. Kwon, "A novel dual-rotor, axial field, fault-tolerant flux-switching permanent magnet machine with high-torque performance," *IEEE Trans. Magn.*, vol. 51, no. 11, pp. 1–4, Jun. 2015.
[10] J. Yan, H. Lin, Y. Huang, H. Liu, and Z. Q. Zhu, "Magnetic field analysis of a novel flux switching transverse flux permanent magnet wind generator with 3-D FEM," in *Proc. Int. Conf. Power Electron. Drive Syst. (PEDS)*, Nov. 2009, pp. 332–335.
[11] W. Ullah, F. Khan, and E. Sulaiman, "Sub-domain modelling and multi-variable optimisation of partitioned PM consequent pole flux switching machines," *IET Electr. Power Appl.*, vol. 14, no. 8, pp. 1360–1369, Aug. 2020.
[12] W. K. Ullah, S. Faisal, U. Erwan, U. Muhammad, and K. Noman, "Analytical validation of novel consequent pole E-core stator permanent magnet flux switching machine," *IET Electr. Power Appl.*, vol. 14, no. 5, pp. 789–796, 2020.
[13] W. Ullah, F. Khan, M. Umair, and B. Khan, "Analytical methodologies for design of segmented permanent magnet consequent pole flux switching machine: A comparative analysis," *COMPEL-Int. J. Comput. Math. Electr. Electron. Eng.*, vol. 40, no. 3, pp. 744–767, Aug. 2021.
[14] W. Ullah, F. Khan, E. Sulaiman, I. Sami, and J.-S. Ro, "Analytical sub-domain model for magnetic field computation in segmented permanent magnet switched flux consequent pole machine," *IEEE Access*, vol. 9, pp. 3774–3783, 2021.
[15] Z. Q. Zhu, Y. Pang, D. Howe, S. Iwasaki, R. Deodhar, and A. Pride, "Analysis of electromagnetic performance of flux-switching permanent-magnet machines by nonlinear adaptive lumped parameter magnetic circuit model," *IEEE Trans. Magn.*, vol. 41, no. 11, pp. 4277–4287, Nov. 2005.
[16] Y. Tang, E. Motoasca, J. J. H. Paulides, and E. A. Lomonova, "Comparison of flux-switching machines and permanent magnet synchronous machines in an in-wheel traction application," *COMPEL-Int. J. Comput. Math. Electr. Electron. Eng.*, vol. 32, no. 1, pp. 153–165, Dec. 2012.
[17] X. Zhu, Z. Shu, L. Quan, Z. Xiang, and X. Pan, "Design and multicondition comparison of two outer-rotor flux-switching permanent-magnet motors for in-wheel traction applications," *IEEE Trans. Ind. Electron.*, vol. 64, no. 8, pp. 6137–6148, Aug. 2017.
[18] W. Hua, H. L. Zhang, M. Cheng, J. Meng, and C. Hou, "An outer-rotor flux-switching permanent-magnet-machine with wedge-shaped magnets for in-wheel light traction," *IEEE Trans. Ind. Electron.*, vol. 64, no. 1, pp. 69–80, Jan. 2017.
[19] X. Li, S. Liu, and Y. Wang, "Design and analysis of a new HTS dual-rotor flux-switching machine," *IEEE Trans. Appl. Supercond.*, vol. 27, no. 4, pp. 1–5, Jun. 2017.
[20] J.-W. Kwon and B.-I. Kwon, "Design of novel high performance dual rotor flux-switching drum winding machine," *J. Electr. Eng. Technol.*, vol. 14, no. 5, pp. 2019–2025, Sep. 2019.
[21] J. Chen, C. V. Nayar, and L. Xu, "Design and finite-element analysis of an outer-rotor permanent-magnet generator for directly coupled wind turbines," *IEEE Trans. Magn.*, vol. 36, no. 5, pp. 3802–3809, Sep. 2000.
[22] E. M. E. Mohamed, "Outer rotor flux-switching permanent magnet generator for direct drive wind energy applications," presented at the Int. Middle-East Power Syst. Conf. (MEPCON). Cairo, Egypt: Ain Shams Univ., 2014.
[23] C. Yu and S. Niu, "Development of a magnetless flux switching machine for rooftop wind power generation," *IEEE Trans. Energy Convers.*, vol. 30, no. 4, pp. 1703–1711, Dec. 2015.
[24] A. Selema, "Development of a three-phase dual-rotor magnetless flux switching generator for low power wind turbines," *IEEE Trans. Energy Convers.*, vol. 35, no. 2, pp. 828–836, Jun. 2020.
[25] M. Popescu, G. Oprina, A. Mitulet, S. Nicolaie, R. Chihaia, A. Nedelcu, M. Mihaiescu, M. Miu, and D. Marin, "Aspects regarding the application of electric generators to wind energy conversion using counter rotating turbines," in *Proc. 8th Int. Symp. Adv. TOPICS Electr. Eng. (ATEE)*, May 2013, pp. 1–4.
[26] D. Violante, L. Famer, C. Munch, and S. Chevailler, "Design of a PM-generator for a straight flow counter-rotating micro-hydro turbine," in *Proc. 19th Eur. Conf. Power Electron. Appl. (EPE ECCE Europe)*, Sep. 2017, pp. P.1–P.10.
[27] Y. Jiang, J. Zhang, and T. Li, "A segmented brushless doubly fed generator for wind power applications," *IEEE Trans. Mag.*, vol. 54, no. 3, pp. 1–4, Mar. 2018.
[28] L. Melcescu, T. Tudorache, O. Craiu, and M. Popescu, "Finite element analysis of a wind generator with two counter-rotating rotors," in *Proc. Int. Conf. Optim. Electr. Electron. Equip. (OPTIM), Int. Aegean Conf. Electr. Mach. Power Electron. (ACEMP)*, May 2017, pp. 408–413.
[29] R. Nasiri-Zarandi, A. Ghaheri, and K. Abbaszadeh, "Thermal modeling and analysis of a novel transverse flux HAPM generator for small-scale wind turbine application," *IEEE Trans. Energy Convers.*, vol. 35, no. 1, pp. 445–453, Mar. 2020.
[30] S. A. Mirnikjoo, K. Abbaszadeh, and S. E. Abdollahi, "Multiobjective design optimization of a double-sided flux switching permanent magnet generator for counter-rotating wind turbine applications," *IEEE Trans. Ind. Electron.*, vol. 68, no. 8, pp. 6640–6649, Aug. 2021.
[31] S. Mirnikjoo, F. Asadi, K. Abbasazdeh, and S. E. Abdollahi, "Effect of rotor topology on the performance of counter-rotating double-sided flux switching permanent magnet generator," *IEEE Trans. Energy Convers.*, early access, Aug. 10, 2021, doi: 10.1109/TEC.2021.3103555.
[32] H. Yang, S. Lyu, Z. Q. Zhu, H. Lin, S. Wang, S. Fang, and Y. Huang, "Novel dual-stator machines with biased permanent magnet excitation," *IEEE Trans. Energy Convers.*, vol. 33, no. 4, pp. 2070–2080, Dec. 2018.
[33] W. Ullah, F. Khan, and S. Hussain, "Investigation of inner/outer rotor permanent magnet flux switching generator for wind turbine applications," *IEEE Access*, vol. 9, pp. 149110–149117, 2021.
[34] W. Ullah, F. Khan, and S. Hussain, "A comparative study of dual stator with novel dual rotor permanent magnet flux switching generator for counter rotating wind turbine applications," *IEEE Access*, vol. 10, pp. 8243–8261, 2022.
[35] T. S. No, J.-E. Kim, J. H. Moon, and S. J. Kim, "Modeling, control, and simulation of dual rotor wind turbine generator system," *Renew. Energy*, vol. 34, no. 10, pp. 2124–2132, Oct. 2009.
[36] N. Bianchi, M. D. Pr, L. Alberti, and E. Fornasiero, *Theory and Design of Fractional-Slot PM Machines*. Italy, Padova: CLEUP, 2007.
[37] J. T. Chen and Z. Q. Zhu, "Winding configurations and optimal stator and rotor pole combination of flux-switching PM brushless ac machines," *IEEE Trans. Energy Convers.*, vol. 25, no. 2, pp. 293–302, Jun. 2010.
[38] A. A. Arkadan, T. M. Hijazi, and B. Masri, "Design evaluation of conventional and toothless stator wind power axial-flux PM generator," *IEEE Trans. Magn.*, vol. 53, no. 6, pp. 1–4, Jun. 2017.
[39] L. E. Somesan, K. Hameyer, E. Padurariu, I.-A. Viorel, and C. Martis, "Sizing-designing procedure of the permanent magnet flux-switching machine based on a simplified analytical model," in *Proc. 13th Int. Conf. Optim. Electr. Electron. Equip. (OPTIM)*, May 2012, pp. 653–658.
[40] W. Ullah, F. Khan, E. Sulaiman, and M. Umair, "Torque characteristics of high torque density partitioned PM consequent pole flux switching machines with flux barriers," *CES Trans. Electr. Mach. Syst.*, vol. 4, no. 2, pp. 130–141, Jun. 2020.

WASIQ ULLAH (Graduate Student Member, IEEE) was born in Peshawar, Khyber Pakhtunkhwa, Pakistan, in 1995. He received the B.S. and M.S. degrees in electrical (power) engineering from COMSATS University Islamabad (Abbottabad Campus), Abbottabad, Pakistan, in 2018 and 2020, respectively, where he is currently pursuing the Ph.D. degree in electrical (power) engineering.

Since 2018, he has been a Research Associate with the Electric Machine Design Research Laboratory. His research interests include analytical modelling, design analysis and optimization of permanent magnet flux switching machines, linear flux switching machines, hybrid excited flux switching machines, novel consequent pole flux switching machines for high-speed brushless AC applications, and flux switching generators for counter-rotating wind turbines applications.

Mr. Ullah is a member of IEEE-IES Electrical Machines Technical Committee and the Pakistan Engineering Council. He is basically from Afghanistan and serve as a Reviewer for IEEE Access, *IET Electric Power Application*, *Energies* (MDPI), and 2022 IEEE Energy Conversion Congress and Exposition (ECCE 2022).

FAISAL KHAN (Member, IEEE) was born in Charsadda, Khyber Pakhtunkhwa, Pakistan, in 1986. He received the B.S. degree in electronics engineering and the M.S. degree in electrical engineering from COMSATS University Islamabad (Abbottabad Campus), Pakistan, in 2009 and 2012, respectively, and the Ph.D. degree in electrical engineering from Universiti Tun Hussein Onn Malaysia, Malaysia, in 2017.

From 2010 to 2012, he was a Lecturer with the University of Engineering and Technology, Abbottabad, Pakistan. Since 2017, he has been an Assistant Professor with the Electrical and Computer Engineering Department, COMSATS University Islamabad (Abbottabad Campus). He is the author of more than 100 publications, one patent, and received multiple research awards. His research interests include design and analysis of flux-switching machines, synchronous machines, and DC machines.

Dr. Khan is a member of IEEE-IES Electrical Machines Technical Committee and the Pakistan Engineering Council.

SHAHID HUSSAIN (Graduate Student Member, IEEE) was born in Swabi, Khyber Pakhtunkhwa, Pakistan. He received the B.S. degree in electrical (power) engineering from COMSATS University Islamabad, Abbottabad Campus, Abbottabad, Pakistan, in 2019, where he is currently pursuing the M.S. degree in electrical (power) engineering. He has been a Research Assistant with the Electric Machine Design Research Laboratory, since 2020. His research interests include design analysis, optimization and experimental validation of modular, and complementary fault tolerant field excited linear flux switching machines for long stroke application. He is a member of the Pakistan Engineering Council.